

Weyl nodes in periodic structures of superconductors and spin active materials

Ahmet Keles^{1,2} and Erhai Zhao²

¹*Department of Physics and Astronomy, University of Pittsburgh, Pittsburgh, PA 15260*

²*Department of Physics and Astronomy, George Mason University, Fairfax, VA 22030*

Motivated by recent progress in epitaxial growth of proximity structures of s -wave superconductors (S) and spin-active materials (M), we show that the periodic structure of S and M can behave effectively as a superconductor with pairs of point nodes, near which the low energy excitations are Weyl fermions. A simple toy model, where M is described by a Kronig-Penney potential with both spin-orbit coupling and exchange field, is proposed and solved to obtain the phase diagram of the nodal structure, the spin texture of the Weyl fermions, as well as the zero energy surface states in the form of open Fermi lines (“Fermi arcs”). Going beyond the simple model, a lattice model with alternating layers of S and magnetic Z_2 topological insulators (M) is solved. The calculated spectrum confirms previous prediction of Weyl nodes based on tunneling Hamiltonian of Dirac electrons. Our results provide further evidence that periodic structures of S and M are well suited for engineering gapless topological superconductors.

The time-honored recipe for discovering new superconductors with interesting pairing symmetries or topological properties is via the synthesis of new materials. In recent years, an alternative approach has been advocated and gained experimental success. It is based on making proximity structures of s -wave superconductor (referred to as S hereafter) and spin active materials (M) such as semiconductors, topological insulators^{1,2} or ferromagnets with spin-orbit and/or exchange coupling. With proper design, the proximity structure can behave effectively as a superconductor with the desired symmetry or topology, at energies below the bulk superconducting gap of S. For example, Fu and Kane³ showed that the interface of a three-dimensional topological band insulator (TI) and an s -wave superconductor is analogous to a spinless $p_x + ip_y$ superconductor that hosts Majorana zero modes at vortex cores. Similar states also arise in proximity structures of S and two dimensional electron gas with Rashba spin-orbit coupling and Zeeman splitting either due to a nearby ferromagnetic insulator or an external magnetic field⁴⁻⁸. In one dimension, e.g., a semiconductor nanowire⁹ or a chain of ferromagnetic atoms deposited on a superconductor¹⁰, Majorana zero modes form at the sample edges. While it remains a challenge to fabricate and control the interface properties, or detect the unequivocal experimental signatures of these states, significant experimental progress has been made in recent years (for an overview, see Refs. 11 and 12).

In this paper, we explore the possibility of realizing gapless topological superconductivity in S-M proximity structures. Specifically, we focus on superconducting states with topologically protected point nodes, i.e., the analogs of the A phase of superfluid ^3He ¹³ and Weyl semimetals¹⁴⁻¹⁶. Such a state was predicted to appear in the superlattice structures of superconductors and magnetic topological insulators by Meng and Balents, and referred to as “Weyl superconductors”¹⁷. The elegant analysis of Ref. 17 is based on an effective Hamiltonian describing the tunneling of the helical Dirac electrons (the surface states of TI) across the layers of TI and S, where the presence of the superconducting pairing potential and

Zeeman field provide a mass to the Dirac electrons. The proposal of Meng and Balents can be viewed as the generalization of the earlier work on Weyl semimetal in the multilayer structures of trivial insulators and magnetic topological insulators¹⁸. One is then led to the following questions: is it feasible to realize Weyl superconductors using materials other than topological insulators; is helical Dirac electron essential?

We answer these questions by considering a simple, idealized model of S-M superlattice. Here M stands for a general spin active material with both spin-orbit coupling and exchange splitting (i.e., both the time reversal and spatial inversion symmetry are broken). We assume, as in Ref. 17, that the M layer is sufficiently thin so that the suppression of superconductivity is not significant and the superconducting phase coherence is maintained across the M layers. This motivates us to approximate the M layers as delta function spin-active potentials, similar to the well known Kronig-Penney model. The band structure of this model is solved to illustrate the reconstruction of the low energy spectrum due to the periodic spin-active potential. We identify parameter regimes where the spectrum has one pair or two pairs of Weyl nodes. We discuss the low energy effective Hamiltonians near the Weyl nodes, and the Fermi line (usually referred to as “Fermi arc”¹⁹) zero energy surface states that manifest the nontrivial topological properties of the superconducting state. This model clearly illustrates that neither TI nor helical Dirac electron is necessary for Weyl nodes to appear in S-M superlattices.

This simple model can be straightforwardly generalized to treat finite thickness of the M layer. It however neglects many microscopic details of the specific materials and the S-TI interface. For the purpose of providing design parameters for Weyl superconductors, it is also desirable to describe the periodic structure by tight binding models defined on discrete lattices. We present such a lattice model for the S-TI superlattice, in which each unit cell consists of a few layers of S and another few layers of magnetized TI with a tunable hopping matrix describing the coupling between the two materials. We

outline a procedure to compute the energy spectrum of the superlattice, and assess the requirements to realize Weyl superconductors with one pair of nodes and two pairs of nodes respectively. Along the way, we briefly review the properties of a single S-TI interface³, and discuss the relation between the Andreev bound states at a single interface²⁰ and the spectrum of multilayer systems.

I. A SIMPLE MODEL FOR S-M SUPERLATTICE

We consider a periodic layered structure of an *s*-wave superconductor (S) and a spin active material (M) extending in the *z* direction as schematically shown in Fig. 1. As far as the low energy excitations are concerned (relative to the bulk superconducting gap Δ), M amounts to a periodic spin-active potential $\hat{V}(z+d) = \hat{V}(z)$, where the hat denotes matrices in spin space. To preserve the superconductivity throughout the whole structure, the M layers should not be too thick so we assume the M layer thickness is much smaller than the period *d*. In this limit, \hat{V} can be modeled by Kronig-Penney potential of the form

$$\hat{V}(\mathbf{k}_{\parallel}, z) = d \sum_n \delta(z - nd) [V_0 + \sum_i V_i(\mathbf{k}_{\parallel}) \hat{\sigma}_i]. \quad (1)$$

Here $\hat{\sigma}$'s are the Pauli matrices in the spin space, $\mathbf{k}_{\parallel} = (k_x, k_y)$ is the transverse momentum which is conserved due to translational invariance on the *xy* plane. Note that the material details of M do not enter in this description, they are encoded in V_0 and V_i which are chosen to reproduce the scattering matrix of electrons by M. The superlattice is then described by the following Hamiltonian in the particle-hole space,

$$\check{\mathcal{H}}(\mathbf{k}_{\parallel}, z) = \begin{bmatrix} \hat{h}_0(\mathbf{k}_{\parallel}, z) & \Delta i \hat{\sigma}_2 \\ -\Delta i \hat{\sigma}_2 & -\hat{h}_0^*(-\mathbf{k}_{\parallel}, z) \end{bmatrix}, \quad (2)$$

with $\hat{h}_0(\mathbf{k}_{\parallel}, z) = (\mathbf{k}_{\parallel}^2 - \partial_z^2)/2m_e - \mu + \hat{V}(\mathbf{k}_{\parallel}, z)$, and the check denotes a matrix in the particle-hole and spin space. Note that we have assumed Δ to be homogeneous, and for $z = nd$, i.e. insides M, the potential \hat{V} dominates all other terms in the Hamiltonian. For simplicity, we shall put $V_0 = 0$. To model M with both spin-orbit coupling and exchange splitting, we assume that \hat{V} takes the form²¹

$$\sum_i V_i(\mathbf{k}_{\parallel}) \hat{\sigma}_i = v_{so}(-k_y \hat{\sigma}_x + k_x \hat{\sigma}_y) + v_z \hat{\sigma}_z, \quad (3)$$

where v_{so} is the strength of Rashba spin-orbit coupling, and v_z is the Zeeman (exchange) field along the *z* direction. Using the periodicity of the Hamiltonian, $\check{\mathcal{H}}(z) = \check{\mathcal{H}}(z + d)$, the band structure can be easily obtained by the expansion of the wave function via Bloch's theorem

$$\check{\Psi}_{\mathbf{k}}(x, y, z) = e^{ik_x x + ik_y y} \sum_G e^{i(k_z + G)z} \check{\Phi}_{\mathbf{k}, G}, \quad (4)$$

where G is reciprocal lattice vector $G = m2\pi/d$ and $m \in \mathbb{Z}$. The generalized Bogliubov-de Gennes (BdG) equation then becomes

$$\sum_{G'} [\check{\mathcal{H}}_0(\mathbf{k}, G) \delta_{G, G'} + \check{\mathcal{V}}(\mathbf{k}_{\parallel})] \check{\Phi}_{\mathbf{k}, G'} = E \check{\Phi}_{\mathbf{k}, G}. \quad (5)$$

Here we have separated the ‘‘unperturbed’’ Hamiltonian

$$\check{\mathcal{H}}_0(\mathbf{k}, G) = \begin{bmatrix} \xi(\mathbf{k}_{\parallel}, k_z + G) & \Delta i \hat{\sigma}_2 \\ -\Delta i \hat{\sigma}_2 & -\xi(\mathbf{k}_{\parallel}, k_z + G) \end{bmatrix}, \quad (6)$$

with $\xi(\mathbf{k}_{\parallel}, k_z + G) = (\mathbf{k}_{\parallel}^2 + (k_z + G)^2)/2m_e - \mu$, and the spin-active ‘‘perturbation’’

$$\check{\mathcal{V}}(\mathbf{k}_{\parallel}) = v_{so}[-k_y \sigma_x + \tau_z \otimes k_x \sigma_y] + v_z \tau_z \otimes \sigma_z \quad (7)$$

with τ_z being the Pauli matrix in the particle-hole space (we will drop the hat for σ when there is no ambiguity).

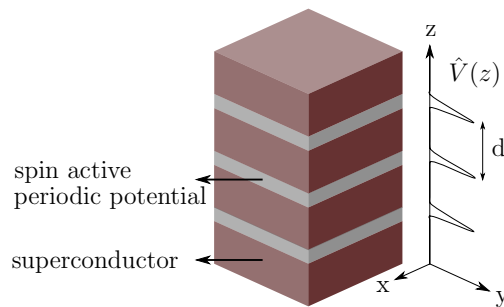


FIG. 1. Schematic of the S-M periodic structure.

The infinite dimensional matrix equation in Eq. 5 can be solved numerically by a truncation, keeping only $|G|$ up to some large enough value of $N\pi/d$, followed by diagonalization to yield the band dispersion $E_{\mathbf{k}}$. This truncation is physically equivalent to introducing a small width to the M layers. Of course one has to check that the low energy spectrum does not depend on N . This model can easily be generalized to the case of M layers with finite thickness. For example, superlattice unit cell can be modeled in a way that the region $z \in [0, d_1]$ is occupied with S (where Δ is constant, \hat{V} is zero) and $z \in [d_1, d]$ is occupied with M (where Δ vanishes but \hat{V} is constant). In this case, both Δ and \hat{V} have off-diagonal matrix elements in G space and the resulting BdG equation is slightly more complicated than Eq. 5.

We are particularly interested in the zero energy solutions of Eq. 5. For this purpose, it is useful to introduce $\check{\phi}_{\mathbf{k}} = \sum_G \check{\Phi}_{\mathbf{k}, G}$ which can be shown to satisfy the following equation;

$$\check{A}_{\mathbf{k}, E} \check{\phi}_{\mathbf{k}} \equiv \left[1 - \sum_G (E - \check{\mathcal{H}}_0(\mathbf{k}, G))^{-1} \check{\mathcal{V}}(\mathbf{k}_{\parallel}) \right] \check{\phi}_{\mathbf{k}} = 0. \quad (8)$$

The matrix inverse is the bare Green function of the bulk superconductor and can be computed analytically. Existence of the zero energy solutions ($E = 0$) at isolated

nodal points on the k_z axis with $\mathbf{k}_{\parallel} = 0$ is equivalent to the existence of a non-trivial solution of Eq. 8 which can be expressed as $\det A_{\mathbf{k},0} = 0$. This equation can be further manipulated analytically to give the following simple equation as the condition of the zero energy solutions;

$$g^2 + f^2 - 1 = 0, \quad (9)$$

where $g = v_z \sum_m \xi_m / (\xi_m^2 + \Delta^2)$, $f = v_z \sum_m \Delta / (\xi_m^2 + \Delta^2)$ and $\xi_m = (k_z + 2\pi m/d)^2 / 2m_e - \mu$. This offers a fast way to scan for Weyl nodes in the parameter space since no numerical diagonalization is required.

Before we present any numerical results, it is worthwhile to develop a qualitative picture of the low energy excitations in such S-M superlattices. Consider the normal state dispersion (turning off superconductivity by setting Δ to zero) in the absence of M. For $\mathbf{k}_{\parallel} = 0$, the low energy excitations are located at large momenta around $k_z \sim \pm k_F$. In the presence of a weak periodic potential \hat{V} , the spectrum of the superlattice structure can be obtained by folding the free dispersion into the first Brillouin zone $k_z \in [-\pi/d, \pi/d]$ which gives a set of Bloch bands, $(k_z + G)^2 / 2m_e$, all being restricted to small momenta since $\pi/d \ll k_F$. The spectrum acquires a gap as Δ is turned on. A finite Zeeman field will split the Andreev bound states formed below the superconducting gap Δ , and push one of the branch towards the zero energy. A non-zero spin-orbit coupling can in principle endow a topologically nontrivial spin structure to these zero energy states. The S-M proximity structure considered here differs from the well studied system of semiconductor nanowires⁶ in its dimensionality. In three dimensions, linear dispersion in the vicinity of the nodes is known to be described by the Weyl Hamiltonian^{13,19}.

II. WEYL NODES

Two representative examples of the low energy spectrum of the S-M superlattice are shown in Fig. 2. We will explicitly show that they correspond to one pair and two pairs of Weyl nodes, respectively. In both cases, we observe a linear energy-momentum dispersion near isolated points $\{\mathbf{k}^0\}$ located on the k_z axis. At any of these diabolical points, the zero energy state is doubly degenerate. Let us label these two degenerate states as $|\Psi_+\rangle$ and $|\Psi_-\rangle$, or $|\pm\rangle$ for short. The low energy physics near the node is described by an effective Hamiltonian which is a 2×2 matrix in the Hilbert space spanned by $|\pm\rangle$ with the general form¹⁹

$$\mathcal{H}(\mathbf{q}) = \frac{1}{2} \mathbf{h}(\mathbf{q}) \cdot \tilde{\boldsymbol{\tau}} = \sum_{i,j=1}^3 v_{ij} q_j \tilde{\tau}_i, \quad \mathbf{q} = \mathbf{k} - \mathbf{k}^0. \quad (10)$$

Here $\tilde{\tau}_i$ are the pseudospin Pauli matrix in the \pm space. The low energy Bogoliubov quasiparticles thus resemble massless chiral fermions (Weyl fermions). The chirality

refers to the locking of the pseudospin with respect to the momentum direction as described by $\mathbf{h}(\mathbf{q})$. The direction of \mathbf{h} , $\hat{h}(\mathbf{q})$, constitutes a mapping from a sphere in the momentum space enclosing the Weyl nodes to a unit sphere in pseudospin space. The topological invariant for this mapping is the winding number¹³

$$\mathcal{N} = \frac{1}{8\pi} \sum_{i,j,k} \epsilon_{ijk} \int d\Omega_k \hat{h} \cdot (\partial_i \hat{h} \times \partial_j \hat{h}) \quad (11)$$

where the integration is over a closed volume containing $q = 0$, and $\partial_j = \partial/\partial q_j$. In the simplest example $\mathbf{h} = \pm \mathbf{q}$, $\mathcal{N} = \pm 1$; and for $v_{ij} = \lambda_i \delta_{ij}$, $\mathcal{N} = \prod_i \text{sign}(\lambda_i)$. Since \mathcal{H} resembles to a spin-1/2 particle in magnetic field, one can define Berry connection and the corresponding flux density¹⁹. Then a Weyl node corresponds to a magnetic monopole with charge \mathcal{N} in the momentum space. For periodic systems, the net flux through the Brillouin zone (BZ) and the net magnetic charge inside the BZ must be zero¹⁹. Therefore Weyl nodes always appear in pairs of opposite charge \mathcal{N} . They are well separated in \mathbf{k} space and topologically stable¹⁹.

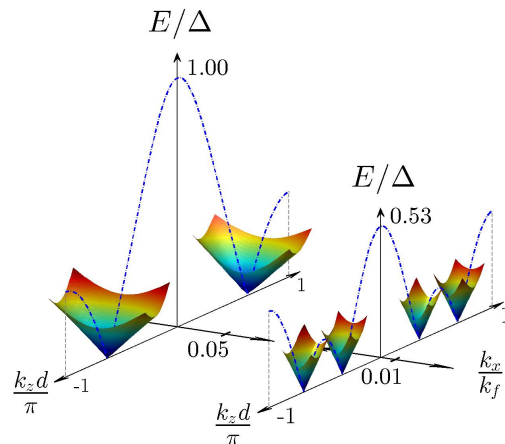


FIG. 2. Weyl nodes in S-M superlattices. Only the lowest eigen energy $E(k_x, k_y = 0, k_z)$ is shown. Blue line is its dispersion along the k_z axis inside the first Brillouin zone $k_z \in [-\pi/d, \pi/d]$. Left panel: single pair of Weyl nodes. The range of k_x is $k_x/k_F \in [-.05, .05]$. $d = 10\pi/k_F$, $v_z = 2.5\Delta$. Right panel: two pairs of Weyl node for $k_x/k_F \in [-.015, .015]$, $d = 9.5\pi/k_F$, $v_z = \Delta$. Here d is the superlattice period, v_z is the strength of Zeeman field and v_{so} is the spin-orbit coupling. We choose $\Delta = 0.05\mu$ and $v_{so} = 5\Delta$.

It is important to conduct the search for zero energy states in the entire momentum space. Fig. 3 shows the energy-momentum dispersion along the k_x axis for fixed $k_z = k_z^0$ for various values of v_{so} . For very small spin-orbit coupling, the slope around $k_x = 0$ is vanishingly small, and there are many other low lying states at larger values of k_x that are sufficiently close to zero energy. These are Andreev bound states (ABS) ubiquitously found in superconducting proximity structures.

For example, for $v_{so} = 0$, the structure reduces to a superconductor-ferromagnet (S-F) superlattice. It is then expected from semiclassical consideration that a series of ABS with finite k_x will be formed between two adjacent F layers. The slope near $k_x = 0$ increases with v_{so} . At the same time, other ABS at finite k_x are increasingly gapped out. For large enough v_{so} , the Weyl nodes on the k_z axis are the only zero energy states. In other words, spin-orbit coupling is crucial for the S-M superlattice to qualify as a Weyl superconductor. Strong spin-orbit coupling is preferred because it gives a steep dispersion around the node, making it well separated from other sub-gap excitations.

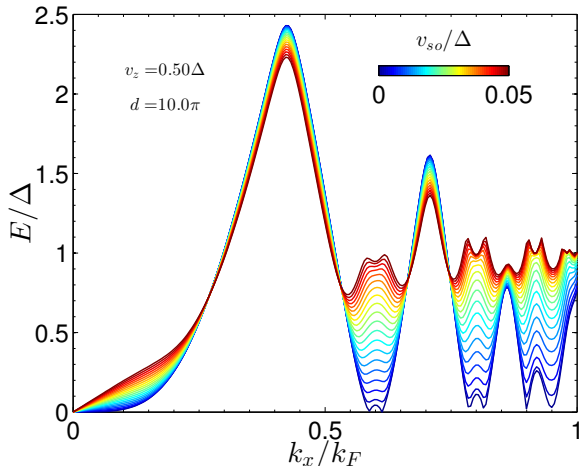


FIG. 3. The dispersion of energy with respect to k_x at the Weyl nodes for different values of spin-orbit coupling v_{so} . The other parameters are identical to the left panel of Fig. 2.

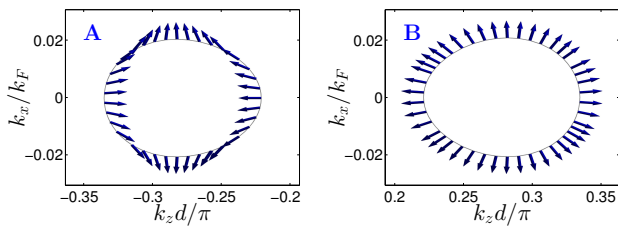


FIG. 4. The pseudospin \mathbf{h} (arrows) on equal energy contours (grey lines) near a pair of Weyl nodes. Note that $k_y = 0$ and $h_x = 0$. To show the (three dimensional) \mathbf{h} vector on the (k_x, k_z) plane, we plot h_z along the k_z axis and h_y along the k_x axis. Panel A is near the node at $-k_z^0$ whereas panel B is near the node at k_z^0 . $\Delta = 0.05\mu$, $v_{so} = 0.5\mu$, $v_z = 0.05\mu$, $d/\pi = 10/k_F$.

We have numerically computed the pseudospin texture near the Weyl nodes. Consider a state $|\tilde{\Psi}_{\mathbf{k}}\rangle$ with positive energy and a momentum \mathbf{k} on one of the cones shown in Fig. 2, and construct a spinor χ by projecting $|\tilde{\Psi}_{\mathbf{k}}\rangle$ onto the $|\tilde{\Psi}_{\pm}\rangle$ basis formed by the zero energy states at the

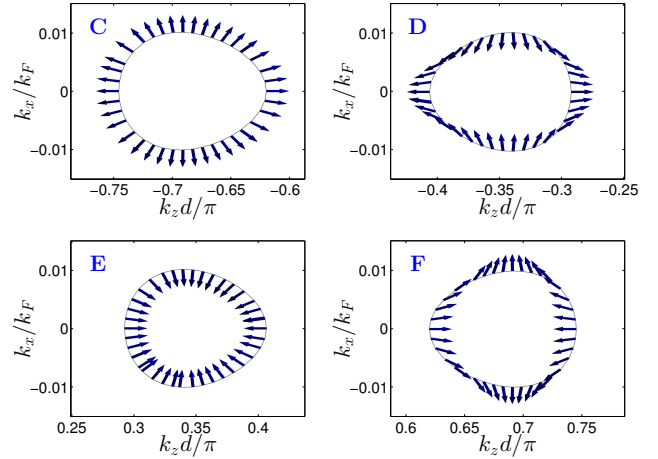


FIG. 5. The pseudospin \mathbf{h} on equal energy contours near two pairs of Weyl nodes, C, D, E, and F. $k_y = 0$ and $h_x = 0$, h_z is along the k_z axis and h_y is along the k_x axis. $\Delta = 0.05\mu$, $v_{so} = 0.5\mu$, $v_z = 0.05\mu$, $d/\pi = 9.5/k_F$.

given node,

$$|\chi\rangle = \begin{pmatrix} u \\ v \end{pmatrix} \equiv \begin{pmatrix} \langle \tilde{\Psi}_+ | \tilde{\Psi}_{\mathbf{k}} \rangle \\ \langle \tilde{\Psi}_- | \tilde{\Psi}_{\mathbf{k}} \rangle \end{pmatrix}. \quad (12)$$

The three components of the \mathbf{h} vector are the expectation values of the corresponding Pauli matrices $\tilde{\tau}_i$ in state $|\chi\rangle$,

$$h_z = \frac{1}{2} (|u|^2 - |v|^2), \quad (13)$$

$$h_x = \text{Re}(u^*v), \quad (14)$$

$$h_y = \text{Im}(u^*v). \quad (15)$$

The result is illustrated in Fig. 4 for the case of single pair of Weyl nodes. The pseudospin texture suggests that

$$\mathcal{H}_{\pm} = v_{\parallel} [q_x \tilde{\tau}_y + q_y \tilde{\tau}_x] \pm v_z q_z \tilde{\tau}_z \quad (16)$$

for the two nodes at $\pm k_z^0$ respectively. Using the formula for \mathcal{N} above, we can rescale q to find their corresponding topological charge $\mathcal{N} = \pm 1$, i.e., the two Weyl nodes have opposite topological charge (chirality). The characteristic spin texture around two pairs of Weyl nodes is illustrated in Fig. 5. We observe that the topological charges of the two nodes on the positive k_z axis, such as E and F, are opposite of each other. The two nodes at mirroring position $\pm k_z^0$, e.g., D and E, also possess opposite charge.

III. FERMI ARC

The Andreev bound states formed at the surface of a Weyl superconductor are very peculiar. The zero energy surface states in the two dimensional momentum space (such as the surface Brillouin zone) take the shape of a continuum line connecting two Weyl nodes of opposite

topological charge. Its topological origin has been discussed in the context of Weyl semimetal^{14,19} and the A phase of ³He^{22,23} and will not be repeated here. Instead we explicitly compute the spectrum of S-M superlattice structures that have a finite width L in the y -direction to demonstrate the Fermi lines. Since the wave function has to vanish at $y = 0$ and $y = L$, we can expand it in sine Fourier series,

$$\check{\Psi}(x, y, z) = e^{ik_x x + ik_z z} \sum_{G, n} \check{\Phi}_{G, n} e^{iGz} \sin\left(\frac{n\pi}{L}y\right). \quad (17)$$

Then the BdG equation becomes

$$\check{H}_0(G, n)\check{\Phi}_{G, n} + \sum_{n', G'} \check{V}_{nn'}\check{\Phi}_{G', n'} = \epsilon\check{\Phi}_{G, n} \quad (18)$$

where we have defined

$$\check{H}_0(G, n) = \begin{bmatrix} \xi(k_x, n, k_z + G) & \Delta i\sigma_2 \\ -\Delta i\sigma_2 & -\xi(k_x, n, k_z + G) \end{bmatrix} \quad (19)$$

with $\xi(k_x, n, k_z + G) = (k_x^2 + k_n^2 + (k_z + G)^2)/2m_e - \mu$, $k_n = n\pi/L$, and $\check{V}_{nn'}(\mathbf{p}) = \delta_{nn'}[-v_{so}k_x\sigma_y + v_z\sigma_z] \otimes \tau_3 + v_{so}\kappa_{nn'}\sigma_x$ with

$$\kappa_{nn'} = \frac{2}{L} \int_0^L dy \sin(k_n y) [-i\partial_y] \sin(k'_n y). \quad (20)$$

In the numerical solution of the BdG equation, Eq. 18, it is important to keep enough k_n .

Fig. 6 shows the calculated finite-slab spectrum for single pair (upper panel) and two pairs (lower panel) of Weyl nodes. In the former case, a continuous line of zero energy states is formed along the k_z axis connecting the bulk Weyl node at k_z^0 to that at $-k_z^0$. These Fermi arc (in this case just a straight line) states are absent in the bulk spectrum and correspond to the surface states at $y = 0$ and L . In fact, a very small gap is visible due to the hybridization of the two surfaces that are of finite distance L apart. In the latter case, the Fermi arc connects the two bulk Weyl nodes on the positive k_z axis. (There is another arc along the negative k_z axis, which is not shown.) This is in accordance with the topological charge of the nodes found above from the spin texture.

IV. PHASE DIAGRAM

The spin texture and the Fermi arc surface states presented above unambiguously established the existence of pairs of Weyl nodes in S-M periodic structures. We have systematically scanned the parameter space of this model and the resultant phase diagram is shown in Fig. 7. Most strikingly, one observes a series of lobes (light gray regions, \mathbb{W}_1) that feature single pair of Weyl nodes, similar to that shown in the left panel of Fig. 2. Roughly speaking, each lobe appears when $k_F d = n\pi$ ($n \in \mathbb{Z}$) and $v_z > \Delta$. The dark black regions (\mathbb{W}_2) represent

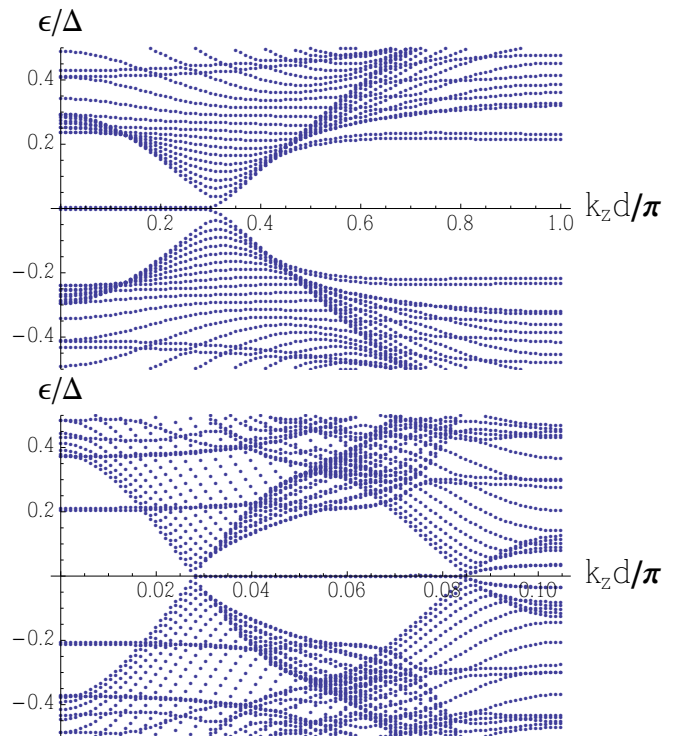


FIG. 6. Fermi arcs on the surface of the S-M superlattice. The plot shows the low energy spectrum $\epsilon(k_x = 0, k_z)$ of a finite slab $y \in [0, L]$. Top panel: the arc connects k_z^0 and $-k_z^0$ (only the positive k_z is shown). $k_F d = 50$, $v_z = 0.6\Delta$. Bottom panel: the Fermi arc along the k_z axis connects two Weyl nodes on the positive k_z axis. $k_F d = 30$, $v_z = 1.1\Delta$. In both cases, $k_F L = 200$, $\mu = 20\Delta$, $v_{so} = \Delta$.

phases with two pairs of Weyl nodes. They also appear as a regular array but are well separated from each other and much smaller in area compared to \mathbb{W}_1 . In fact, \mathbb{W}_2 can be viewed as the overlapping regions of two adjacent \mathbb{W}_1 phases, as seen in the inset of Fig. 7 which shows the details near $d/\pi = 10$. In the rest of the phase diagram (white regions, \mathbb{W}_0), the spectrum is gapped, even through the gap may be numerically small (see for example the spectrum at point A shown in the first sub-panel).

The evolution of the spectrum along a vertical cut in the phase diagram, from point A to point F, is illustrated in the sub-panels of Fig. 7. As v_z is increased at this particular value of d , the lowest branch of the spectrum is pushed down by the increasing Zeeman splitting to touch $E = 0$, entering the \mathbb{W}_2 phase (A→B). With further increase of v_z , the newly born twin of Weyl nodes with opposite charge become increasingly detached from each other, with one heading towards $k_z = 0$ and the other towards the BZ boundary. The latter gets gapped out once it reaches the BZ boundary where it annihilates with its mirror image living on the negative k_z axis, thus marking the transition from the \mathbb{W}_2 phase to the \mathbb{W}_1 phase (C→D). Further increase of v_z will push the spectrum away from $E = 0$, and the two Weyl nodes of opposite charge annihilate with each other at $k_z = 0$, leaving be-

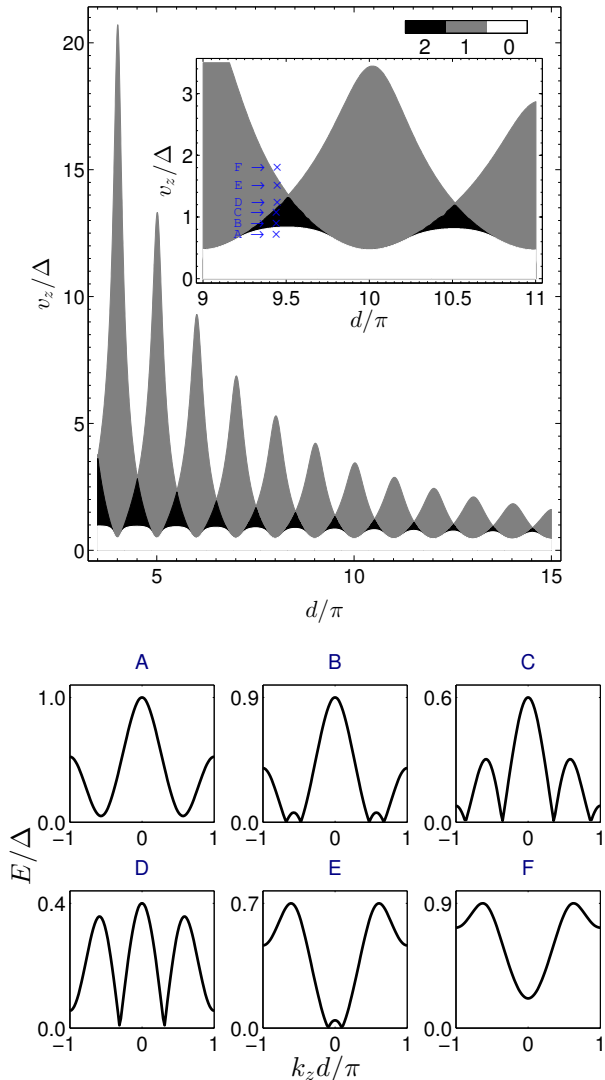


FIG. 7. Top: Phase diagram of the nodal structure of the S-M superlattice as a function of superlattice spacing d and Zeeman field v_{so} in the regime of sufficiently strong spin-orbit coupling. The shaded (light grey) region corresponds to one pair of Weyl nodes, and the dark black region corresponds to two pairs of Weyl nodes. The spectrum is gapped in the white region. $\Delta = 0.05\mu$, the superlattice period d is measured in $1/k_F$. Inset: zoom-in of the region around $dk_F/\pi = 10$. The energy spectra (the lowest energy) along a vertical cut, from point A to point F, are shown in the bottom panel.

hind a vacuum (E→F).

V. LATTICE MODEL

Now we turn to S-M heterostructures described by tight binding Hamiltonians defined on discrete lattices. Compared to the continuum model above, the lattice model can sometimes offer more realistic descriptions of

the material-specific properties, especially regarding the coupling between S and M, and in the limit where the thickness of S and M is comparable to each other. As a result, the lattice model can potentially provide more quantitative predictions of the design parameters of Weyl superconductors. We will illustrate this approach by focusing on the superconductor-magnetic topological insulator (S-TI) superlattice structure proposed in Ref. 17. In contrast to Ref. 17, however, we start from microscopic models of S and TI instead of the low energy surface degrees of freedom (i.e., the Dirac electrons).

For simplicity, we model both S and TI on cubic lattice with lattice constant a . Each unit cell of the superlattice consists of N_S layers of S and N_T layers of TI stacked along the z direction. Let i be the layer index, the eigenvalue problem has a tri-diagonal structure

$$T_{i-1,i}\Psi_i + T_{i,i+1}\Psi_{i+1} = (E - H_i)\Psi_i. \quad (21)$$

Here $T_{i,i+1}$ is the hopping matrix coupling layer i to the neighboring layer $i + 1$, H_i is the Hamiltonian for the i -th layer, and Ψ_i is the wave function at the i -th layer. Note that the transverse momentum $\mathbf{k}_{\parallel} = (k_x, k_y)$ is conserved. For each S layer, i.e., $i \in [1, N_S]$,

$$H_i(\mathbf{k}_{\parallel}) = H_S(\mathbf{k}_{\parallel}) = \begin{pmatrix} \xi(\mathbf{k}_{\parallel}) & i\sigma_y\Delta \\ -i\sigma_y\Delta & -\xi^*(-\mathbf{k}_{\parallel}) \end{pmatrix}, \quad (22)$$

where $\xi(\mathbf{k}_{\parallel}) = -2t_s(\cos k_x + \cos k_y) - \mu_s$ and k is measured in units of $1/a$. The hopping between two adjacent S layers is simply

$$T_{i,i+1} = \begin{pmatrix} -t_s & 0 \\ 0 & t_s \end{pmatrix}. \quad (23)$$

For example, we take $t_s = 0.18\text{eV}$, and $\mu = -4t_s$. We consider Bi_2Se_3 as a prime example of 3D Z_2 topological insulators, and model each TI layer by²⁴

$$\hat{h}_M(\mathbf{k}_{\parallel}) = m\hat{\Gamma}_0 + a_2 \sin k_x \hat{\Gamma}_1 + a_2 \sin k_y \hat{\Gamma}_2 + v_z \hat{\sigma}_3 \otimes \hat{1}, \quad (24)$$

where $m(\mathbf{k}_{\parallel}) = M - 2b_1 + 2b_2(\cos k_x + \cos k_y - 2)$. We choose the basis $(|p_+ \uparrow\rangle, |p_+ \downarrow\rangle, |p_- \uparrow\rangle, |p_- \downarrow\rangle)$, where p_{\pm} labels the hybridized p_z orbital with even (odd) parity²⁵. The Gamma matrices are defined as $\hat{\Gamma}_0 = \hat{\tau}_3 \otimes \hat{1}$, $\hat{\Gamma}_i = \hat{\tau}_1 \otimes \hat{\sigma}_i$, with $\hat{\tau}_i$ ($\hat{\sigma}_i$) being the Pauli matrices in the orbital (spin) space. v_z is the Zeeman splitting for magnetically doped Bi_2Se_3 ²⁶⁻²⁸. The coupling between two adjacent TI layers is given by

$$\hat{t}_M = b_1 \hat{\Gamma}_0 - \frac{i}{2} a_1 \hat{\Gamma}_3. \quad (25)$$

The isotropic version of \hat{h}_M and \hat{t}_M , with $a_1 = a_2$, $b_1 = b_2$, was proposed by Qi et al as a minimal model for 3D topological insulators²⁹. To mimic Bi_2Se_3 , we set the lattice spacing $a = 5.2\text{\AA}$, which gives the correct unit cell volume, and $a_i = A_i/a$, $b_i = B_i/a^2$ for $i = 1, 2$. The numerical values of M , A_i , B_i are given in Ref. 25. With these parameters, our model yields the correct band gap

and surface dispersion, it also reduces to the continuum $\mathbf{k} \cdot \mathbf{p}$ Hamiltonian (the Bernevig-Hughes-Zhang model) in the small k limit²⁵, aside from a topologically trivial $\epsilon_0(\mathbf{k})$ term. To describe the superconducting proximity effect, we have to generalize the TI hamiltonian above into the particle-hole space. For $i \in [N_S + 1, N_S + N_T]$,

$$H_i(\mathbf{k}_{\parallel}) = \begin{pmatrix} \hat{h}_M(\mathbf{k}_{\parallel}) & 0 \\ 0 & -\hat{h}_M^*(-\mathbf{k}_{\parallel}) \end{pmatrix}, \quad (26)$$

and accordingly,

$$T_{i,i+1} = \begin{pmatrix} \hat{t}_M & 0 \\ 0 & -\hat{t}_M^* \end{pmatrix}. \quad (27)$$

Finally, the hopping from S to TI is a 4×8 matrix,

$$T_{N_S, N_S+1} = \begin{pmatrix} \hat{t}_{SM}(\mathbf{k}_{\parallel}) & 0 \\ 0 & -\hat{t}_{SM}^*(-\mathbf{k}_{\parallel}) \end{pmatrix} \quad (28)$$

with

$$\hat{t}_{SM}(\mathbf{k}_{\parallel}) = \begin{pmatrix} J_+ & 0 & J_- & 0 \\ 0 & J_+ & 0 & J_- \end{pmatrix}. \quad (29)$$

Here J_{\pm} is the overlap integral between the p -orbital p_{\pm} of TI and the s -like orbital of S. For simplicity, we assume the spin is conserved during the hopping, and from the orbital symmetry, $J_+ = -J_- = J$ where J can be tuned from weak to strong²⁴. Small J mimics a large tunneling barrier between S and TI, while large J describes good contact, i.e., strong coupling between S and TI.

A standard lattice Fourier transform from the layer index i to quasi momentum k_z inside the reduced Brillouin zone, $[-\pi/Na, \pi/Na]$ with $N = N_S + N_T$, gives each $T_{i,i+1}$ a phase factor $e^{ik_z a}$. The Hamiltonian of one unit cell of the superlattice is a matrix of the size $4N_S + 8N_T$ subject to periodic boundary conditions. Then a numerical diagonalization yields the band structure $E(k_x, k_y, k_z)$ of the S-TI superlattice.

VI. ANDREEV BOUND STATES AT THE S-TI INTERFACE

Before discussing the S-TI multilayer system, it is worthwhile to first consider the spectral properties of a single S-TI interface which have been studied extensively since the pioneer work of Fu and Kane³. Comparison with these known results will serve as a critical check of our lattice model presented above. It also establishes the connection between the microscopic model here and the effective model of Fu and Kane for the S-TI interface³, as well as that of Meng and Balents for the S-TI superlattice¹⁷.

The spectrum of a single S-TI interface can be conveniently extracted from our lattice model by taking various limits. Firstly, by setting $J = 0$ and $v_z = 0$ (but keeping finite Δ), the low energy spectrum reduces to the

surface states of the topological insulator. As the thickness N_T is reduced, the linear Dirac spectrum acquires a gap due to the hybridization between two TI surfaces³⁰. For example, the gap is around 0.012eV when $N_T = 8$.

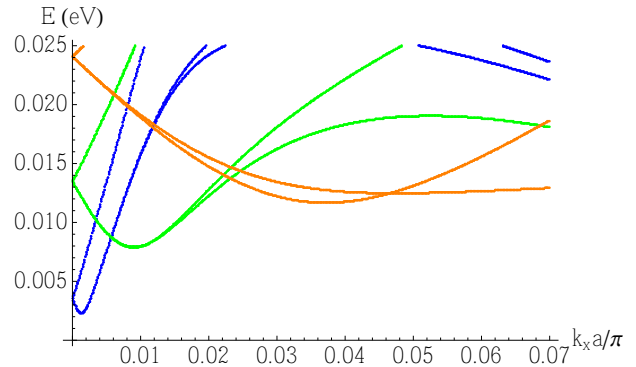


FIG. 8. Andreev bound states at the S-TI interface. $N_S = N_T = 20$, $k_y = k_z = 0$. The blue, green, and red curves are for $J/t_s = 0.2, 0.5, 1$ respectively. Here $v_z = 0$, $\Delta = 14\text{meV}$, $t_s = 0.18\text{eV}$, and $\mu = -4t_s$.

Secondly, by setting $v_z = 0$ and keeping N_T and N_S large, the low energy spectrum $E(k_x, k_y, k_z = 0)$ reduces to that of a single S-TI interface, since all the interfaces are sufficiently far apart and essentially decoupled from each other. Note that in this limit, the BZ is very small, and the dispersion along k_z is negligible so we set $k_z = 0$. Fig. 8 shows the evolution of the sub-gap spectrum as J is increased from the tunneling to the strong coupling limit. In each case, the dispersion of the sub-gap modes can be fit well by formula $E(\mathbf{k}_{\parallel}) = \sqrt{\Delta_s^2 + (v_s |\mathbf{k}_{\parallel}| \pm \mu_s)^2}$ which follows from Fu and Kane's phenomenological model³,

$$H_{FK}(\mathbf{k}_{\parallel}) = \begin{pmatrix} h_s(\mathbf{k}_{\parallel}) & i\sigma_y \Delta_s \\ -i\sigma_y \Delta_s & -h_s^*(-\mathbf{k}_{\parallel}) \end{pmatrix}, \quad (30)$$

where h_s describes the helical Dirac electrons^{3,25},

$$h_s(\mathbf{k}_{\parallel}) = -\mu_s + v_s(\sigma_x k_y - \sigma_y k_x). \quad (31)$$

This suggests that the Fu-Kane model is valid in a broad range of coupling strength between S and TI. Yet, as clearly seen in Fig. 8, the effective parameters (μ_s, Δ_s, v_s) in H_{FK} depend sensitively on J . They may get strongly renormalized from their respective nominal values estimated from the bulk parameters by the proximity effect (the coupling to S). For device applications, e.g. for the generation and manipulation of Majorana zero modes, a large Δ_s and thus a strong S-TI coupling is preferred. In this limit, it is more natural to think of the interface state as the Andreev bound state which penetrates into the superconductor over the coherence length but decays rapidly (over a distance on the atomic scale) in the TI²⁰. The lattice calculation presented here is in agreement with the wave function calculation of Lababidi and Zhao in Ref. 20 and the Green function calculation of Grein et al in Ref. 31.

Thirdly, v_z can be easily incorporated into the Fu-Kane Hamiltonian. For a single S-TI interface, it opens up a Zeeman gap at $\mathbf{k}_{\parallel} = 0$. Using this as the starting point, Meng and Balents¹⁷ analyzed the effective Hamiltonian of the S-TI superlattice and arrived at a very clean phase diagram in the plane of v_z and Δ .

VII. WEYL FERMIONS

In search of Weyl nodes within our microscopic lattice model, we shall focus on “ideal” conditions provided that they seem experimentally feasible. High temperature superconductor (BSCCO) in proximity to Bi_2Se_3 was reported to induce a gap of 15meV, and the pairing symmetry was postulated to be s -wave because no d -wave nodes were observed^{32,33}. In comparison, the gap of Bi_2Se_3 grown on NbSe_3 is on the order of meV³⁴. We will consider a fairly large gap $\Delta = 14\text{meV}$. The Zeeman field v_z can exceed the value of Δ . For example, chromium-doped $\text{Bi}_2(\text{Se}_x\text{Te}_{1-x})_3$ has an exchange gap of 40meV²⁸, and Bi_2Se_3 doped with Mn^{26,35} develops an exchange gap ranging from 10 to 60 meV. As to the number of layers for each materials, we will consider for example $N_S = 5$, $N_T = 3$ which gives a large BZ, allowing k_z to have significant dispersion. Certain natural multilayer heterostructures (not superconducting) of TI such as $(\text{PbSe})_5(\text{Bi}_2\text{Se}_3)_{3m}$ have been reported³⁶. Epitaxial growth of TI films with 1 to 12 quintuple layers on superconducting substrate has been successfully demonstrated³⁷. Also the superconductor BaBiO_3 with $T_c \sim 30\text{K}$ was predicted to turn into a TI upon electron doping³⁸. This implies that the S-TI superlattice may even be realized based on a single compound by modulated electric or chemical doping.

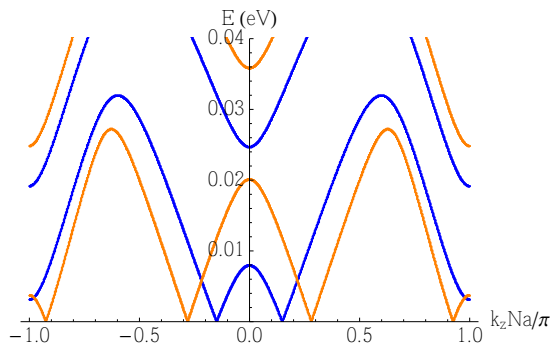


FIG. 9. One pair versus two pairs of Weyl nodes in the S-TI superlattice. The blue (orange) spectrum corresponds to $v_z = 3\Delta$ (5Δ). $N_S = 5$, $N_T = 3$, with $J = 0.7t_s$, $t_s = 0.18\text{eV}$, $\Delta = 14\text{meV}$.

Fig. 9 shows the low energy part of $E(k_x = k_y = 0, k_z)$ for $v_z = 3\Delta$ (blue) and 5Δ (orange). They have one pair and two pairs of Weyl nodes on the k_z axis respectively. One can explicitly check that these nodes are the only zero energy states within the reduced BZ, and the energy

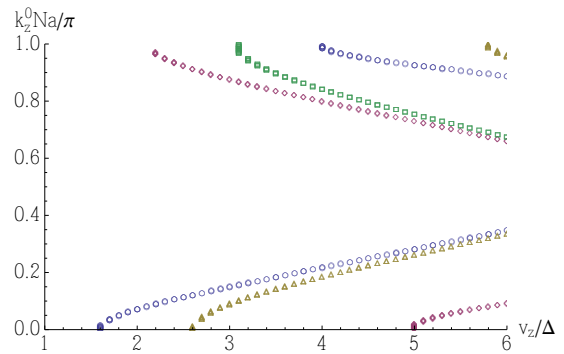


FIG. 10. The number and location of Weyl nodes in the S-TI superlattice as functions of the Zeeman field v_z . The circle, diamond, triangle, and square are for $N_S = 5, 7, 9, 11$ respectively. $N_T = 3$ with $J = 0.7t_s$, $t_s = 0.18\text{eV}$, $\Delta = 14\text{meV}$.

E is indeed linear in $\mathbf{k} - \mathbf{k}^0$. Fig. 10 summarizes the location (and number) of the Weyl nodes on the positive k_z axis as the Zeeman field v_z is increased. The phases and phase boundary can be easily read off from Fig. 10. Take $N_S = 5$ (the empty circle) for example, for $v_z < 1.6\Delta$, the spectrum is gaped and the systems is in phase \mathbb{W}_0 . For $v_z \in [1.6\Delta, 4\Delta]$, there is only one node on the positive k_z axis. And the node moves away from $k_z = 0$ as v_z is increased. This is phase \mathbb{W}_1 . For $v_z > 4\Delta$, a second nodal point appears at the BZ boundary $k_z = \pi/(Na)$. The system enters the \mathbb{W}_2 phase. Overall, the evolution of the nodal structure here is similar to that of the continuum model discussed above. Fig. 10 also compares the phases for increasing number of superconducting layers. As a general trend, the critical v_z required for the $\mathbb{W}_{1,2}$ to appear increases with N_S . In the limit of large N_S , the dispersion along k_z becomes very flat.

VIII. CONCLUDING REMARKS

We have presented two complementary approaches to model and compute the properties of S-M superlattice structures. The first approach is based on a simple continuum model where M is described by periodic spin active potentials that are spatially thin compared to the thickness of the superconductor, and accordingly, the size of the unit cell can be larger than the superconducting coherence length. The second approach is based on a tight binding lattice model describing alternative layers of S and TI, both of which can be only of several layers thick with a tunable coupling strength between the two materials. In both models, we find phases that have one pair or two pairs of Weyl nodes. Together with previous results based on tunneling Hamiltonians¹⁷, our study unambiguously establishes that (a) S-M periodic structures can behave as Weyl superconductors at low energies; and (b) for this to occur, neither topological insulators nor Dirac electrons are necessary, only the right combination

of spin-orbit coupling and Zeeman splitting are required. These observations generalize the proposals of realizing gapped topological superconductors featuring Majorana zero modes in one and two dimensions⁴⁻⁸ to gapless topological superconductors in three dimensions using periodic structures of S and M. We hope that the theoretical analysis presented here can stimulate experimental work to explore these ideas.

The emergence of Weyl fermions at low energies out of the vacuum of a conventional *s*-wave superconductor is quite striking. While these low energy quasiparticles can be viewed as the Andreev bound states formed at the S-M interface dispersing with k_z and crossing zero energy at isolated \mathbf{k} points, they are located in \mathbf{k} space near $\mathbf{k} = 0$ (for $k_F d \gg 1$), instead of being around the original Fermi surface $|\mathbf{k}| = k_F$. In other words, the spectral weight is transferred not only from high to low energy,

but also from high to low momentum, by the presence of the periodic spin active potential. In this paper we have only considered one dimensional S-M superlattice structures. It is very likely that equally interesting phenomena may rise for “metamaterials” of superconductors and spin active materials that have more complicated periodic structures in even higher dimensions.

ACKNOWLEDGMENTS

This work is supported by AFOSR FA9550-12-1-0079 and NSF PHY-1205504. We thank Matthias Eschrig, Mahmoud Lababidi, and Sungkit Yip for stimulating discussions. We also acknowledge the Institute for Nuclear Theory at the University of Washington for its hospitality (INT-15-1 workshop) and the Department of Energy for partial support during the completion of this work.

-
- ¹ M. Z. Hasan and C. L. Kane, *Rev. Mod. Phys.* **82**, 3045 (2010).
 - ² X.-L. Qi and S.-C. Zhang, *Rev. Mod. Phys.* **83**, 1057 (2011).
 - ³ L. Fu and C. L. Kane, *Phys. Rev. Lett.* **100**, 096407 (2008).
 - ⁴ J. D. Sau, R. M. Lutchyn, S. Tewari, and S. Das Sarma, *Phys. Rev. Lett.* **104**, 040502 (2010).
 - ⁵ R. M. Lutchyn, J. D. Sau, and S. Das Sarma, *Phys. Rev. Lett.* **105**, 077001 (2010).
 - ⁶ J. Alicea, *Phys. Rev. B* **81**, 125318 (2010).
 - ⁷ Y. Oreg, G. Refael, and F. von Oppen, *Phys. Rev. Lett.* **105**, 177002 (2010).
 - ⁸ A. C. Potter and P. A. Lee, *Phys. Rev. B* **83**, 184520 (2011).
 - ⁹ V. Mourik, K. Zuo, S. M. Frolov, S. R. Plissard, E. P. A. M. Bakkers, and L. P. Kouwenhoven, *Science* **336**, 1003 (2012).
 - ¹⁰ S. Nadj-Perge, I. K. Drozdov, J. Li, H. Chen, S. Jeon, J. Seo, A. H. MacDonald, B. A. Bernevig, and A. Yazdani, *Science* **346**, 602 (2014).
 - ¹¹ C. Beenakker, *Annual Review of Condensed Matter Physics* **4**, 113 (2013).
 - ¹² J. Alicea, *Reports on Progress in Physics* **75**, 076501 (2012).
 - ¹³ G. Volovik, *The universe in a helium droplet* (Oxford University Press New York, 2009).
 - ¹⁴ X. Wan, A. M. Turner, A. Vishwanath, and S. Y. Savrasov, *Phys. Rev. B* **83**, 205101 (2011).
 - ¹⁵ K.-Y. Yang, Y.-M. Lu, and Y. Ran, *Phys. Rev. B* **84**, 075129 (2011).
 - ¹⁶ P. Delplace, J. Li, and D. Carpentier, *Europhysics Letters* **97**, 67004 (2012).
 - ¹⁷ T. Meng and L. Balents, *Phys. Rev. B* **86**, 054504 (2012).
 - ¹⁸ A. A. Burkov and L. Balents, *Phys. Rev. Lett.* **107**, 127205 (2011).
 - ¹⁹ O. Vafek and A. Vishwanath, *Annual Review of Condensed Matter Physics* **5**, 83 (2014).
 - ²⁰ M. Lababidi and E. Zhao, *Phys. Rev. B* **83**, 184511 (2011).
 - ²¹ J. Michelsen and R. Grein, (2012), [arXiv:1208.1090 \[cond-mat.supr-con\]](https://arxiv.org/abs/1208.1090).
 - ²² Y. Tsutsumi, M. Ichioka, and K. Machida, *Phys. Rev. B* **83**, 094510 (2011).
 - ²³ M. A. Silaev and G. E. Volovik, *Phys. Rev. B* **86**, 214511 (2012).
 - ²⁴ E. Zhao, C. Zhang, and M. Lababidi, *Phys. Rev. B* **82**, 205331 (2010).
 - ²⁵ H. Zhang, C.-X. Liu, X.-L. Qi, X. Dai, Z. Fang, and S.-C. Zhang, *Nat Phys* **5**, 438 (2009).
 - ²⁶ Y. L. Chen, J.-H. Chu, J. G. Analytis, Z. K. Liu, K. Igarashi, H.-H. Kuo, X. L. Qi, S. K. Mo, R. G. Moore, D. H. Lu, M. Hashimoto, T. Sasagawa, S. C. Zhang, I. R. Fisher, Z. Hussain, and Z. X. Shen, *Science* **329**, 659 (2010).
 - ²⁷ C.-Z. Chang, J. Zhang, X. Feng, J. Shen, Z. Zhang, M. Guo, K. Li, Y. Ou, P. Wei, L.-L. Wang, Z.-Q. Ji, Y. Feng, S. Ji, X. Chen, J. Jia, X. Dai, Z. Fang, S.-C. Zhang, K. He, Y. Wang, L. Lu, X.-C. Ma, and Q.-K. Xue, *Science* **340**, 167 (2013).
 - ²⁸ J. Zhang, C.-Z. Chang, P. Tang, Z. Zhang, X. Feng, K. Li, L.-L. Wang, X. Chen, C. Liu, W. Duan, K. He, Q.-K. Xue, X. Ma, and Y. Wang, *Science* **339**, 1582 (2013).
 - ²⁹ X.-L. Qi, T. L. Hughes, and S.-C. Zhang, *Phys. Rev. B* **78**, 195424 (2008).
 - ³⁰ Y. Zhang, K. He, C.-Z. Chang, C.-L. Song, L.-L. Wang, X. Chen, J.-F. Jia, Z. Fang, X. Dai, W.-Y. Shan, *et al.*, *Nature Physics* **6**, 584 (2010).
 - ³¹ R. Grein, J. Michelsen, and M. Eschrig, *Journal of Physics: Conference Series* **391**, 012149 (2012).
 - ³² E. Wang, H. Ding, A. V. Fedorov, W. Yao, Z. Li, Y.-F. Lv, K. Zhao, L.-G. Zhang, Z. Xu, J. Schneeloch, R. Zhong, S.-H. Ji, L. Wang, K. He, X. Ma, G. Gu, H. Yao, Q.-K. Xue, X. Chen, and S. Zhou, *Nat Phys* **9**, 621 (2013).
 - ³³ P. Zareapour, A. Hayat, S. Y. F. Zhao, M. Kreshchuk, A. Jain, D. C. Kwok, N. Lee, S.-W. Cheong, Z. Xu, A. Yang, G. D. Gu, S. Jia, R. J. Cava, and K. S. Burch, *Nat Commun* **3**, 1056 (2012).
 - ³⁴ M.-X. Wang, C. Liu, J.-P. Xu, F. Yang, L. Miao, M.-Y. Yao, C. L. Gao, C. Shen, X. Ma, X. Chen, Z.-A. Xu, Y. Liu, S.-C. Zhang, D. Qian, J.-F. Jia, and Q.-K. Xue, *Science* **336**, 52 (2012).

- ³⁵ S.-Y. Xu, M. Neupane, C. Liu, D. Zhang, A. Richardella, L. Andrew Wray, N. Alidoust, M. Leandersson, T. Balasubramanian, J. Sanchez-Barriga, O. Rader, G. Landolt, B. Slomski, J. Hugo Dil, J. Osterwalder, T.-R. Chang, H.-T. Jeng, H. Lin, A. Bansil, N. Samarth, and M. Zahid Hasan, *Nat Phys* **8**, 616 (2012).
- ³⁶ K. Nakayama, K. Eto, Y. Tanaka, T. Sato, S. Souma, T. Takahashi, K. Segawa, and Y. Ando, *Phys. Rev. Lett.* **109**, 236804 (2012).
- ³⁷ J.-P. Xu, C. Liu, M.-X. Wang, J. Ge, Z.-L. Liu, X. Yang, Y. Chen, Y. Liu, Z.-A. Xu, C.-L. Gao, D. Qian, F.-C. Zhang, and J.-F. Jia, *Phys. Rev. Lett.* **112**, 217001 (2014).
- ³⁸ B. Yan, M. Jansen, and C. Felser, *Nat Phys* **9**, 709 (2013).